



**Metal-Organic Frameworks for Artificial Photosynthesis and Photocatalysis**

Journal:	<i>Chemical Society Reviews</i>
Manuscript ID:	CS-REV-03-2014-000103.R1
Article Type:	Review Article
Date Submitted by the Author:	17-Apr-2014
Complete List of Authors:	Lin, Wenbin; University of Chicago, Department of Chemistry Zhang, Teng; Univ of Chicago, Dept of Chem

## ARTICLE

# Metal-Organic Frameworks for Artificial Photosynthesis and Photocatalysis

Cite this: DOI: 10.1039/x0xx00000x

Teng Zhang and Wenbin Lin\*

Received 00th January 2012,  
Accepted 00th January 2012

DOI: 10.1039/x0xx00000x

www.rsc.org/

Solar energy is an alternative, sustainable energy source for the mankind. Finding a convenient way to convert sunlight energy into chemical energy is a key step towards realizing large-scale solar energy utilization. Owing to their structural regularity and synthetic tunability, metal-organic frameworks (MOFs) provide an interesting platform to hierarchically organize light-harvesting antenna and catalytic centers to achieve solar energy conversion. Such photo-driven catalytic processes not only play a critical role in the solar to chemical energy conversion scheme, but also provide a novel methodology for the synthesis of fine chemicals. In this review, we summarize fundamental principles of energy transfer and photocatalysis and overview the latest progress on energy transfer, light-harvesting, photocatalytic proton and CO<sub>2</sub> reduction, and water oxidation using MOFs. The applications of MOFs on organic photocatalysis and degradation of model organic pollutants are also discussed.

## Introduction

With increasing global energy demand and dwindling fossil fuel supplies, finding alternative and sustainable energy sources has become one of the most important and challenging tasks humanity has ever had to tackle. Owing to the unlimited and sustainable energy influx from the Sun, solar energy has been proposed as the most promising alternative energy source for human consumption. Great efforts have been devoted to solar energy harvesting with various strategies including photovoltaics, photoelectrochemical cells, and others, in the past few decades.<sup>1-4</sup> In particular, photo-driven, thermodynamically uphill ( $\Delta G > 0$ ) reactions are ideal for harvesting and storing sunlight energy in the form of chemical fuels.<sup>5-7</sup> Compared to electric-based energy sources such as supercapacitors or batteries, chemical fuels are of much higher energy density, more convenient for transportation and storage, and suitable for applications under extreme conditions. In addition, large scale production of solar fuels from carbon dioxide reduces the amount of carbon dioxide, one of the most important greenhouse gases, in the atmosphere.

Green plants have evolved over eons to harvest solar energy and use the harvested energy to convert carbon dioxide and water into carbohydrates via a thermodynamically uphill transformation known as photosynthesis. Inspired by the natural photosynthesis, researchers have developed artificial systems and devices with inorganic and organic materials to perform similar photochemical reactions. The first example of artificial photosynthesis was reported by Fujishima and Honda in 1972, in which water splitting was achieved under UV radiation with TiO<sub>2</sub>.<sup>8</sup> Many different materials and devices have since been

demonstrated for artificial photosynthesis,<sup>4, 9-12</sup> yet it still remains a great challenge to develop a cheap and stable system with high efficiency in sunlight utilization and rapid production of solar fuels.

Chemists have also developed a variety of molecular dyes and catalysts in order to mimic the natural photosynthesis system by performing photo-driven proton or CO<sub>2</sub> reduction reactions.<sup>13-16</sup> Three fundamental steps are needed to convert solar energy to chemical energy: sunlight absorption by photosensitizers to create charge-separated excited states, generation of redox equivalents and their migration to reactive centers, and reduction and oxidation half reactions with the redox equivalents (electrons and holes) at the catalytic centers. In molecular systems, photo-driven water splitting or CO<sub>2</sub> reduction is typically explored in the form of half reactions by using a sacrificial reductant. This strategy only examines one or two of the three fundamental steps listed above. Figure 1 shows a typical two-component photocatalytic system composed of a photosensitizer (PS) and a catalyst (cat) for proton reduction in the presence of a sacrificial reductant.<sup>14</sup> Many different designs have also been developed to assemble the PS and cat components as covalent-bonded dimers, supramolecular assemblies, or polymers,<sup>17-19</sup> but the application of these systems is greatly limited by the challenges involved in multi-step syntheses of these systems.

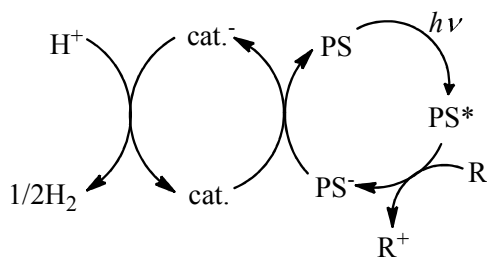


**Figure 1.** A schematic diagram of a two-component photocatalytic system for proton reduction. A sacrificial reductant is needed in such a two-component system, and the overall reaction is typically thermodynamically downhill.

Although many molecular and supramolecular systems have been designed to carry out individual steps, there is no known strategy to hierarchically integrate all of the components in a single material to perform artificial photosynthesis without relying on sacrificial reagents. As a new family of inorganic-organic hybrid supramolecular materials, metal-organic frameworks (MOFs) serve as an interesting platform to design and study artificial photosynthetic systems. MOFs can in principle contain photosensitizers and catalytic centers in a single solid and provide the structural organization to integrate the three fundamental steps of artificial photosynthesis into a single material.

In plant cells, membrane-bounded chromophores assemble into a network that efficiently absorb sunlight to generate excited states and move excited states to a charge separation center, at which photo-induced charge separation takes place. Hundreds of chromophores work cooperatively and make efficient use of sunlight to drive the thermodynamically uphill photosynthesis.<sup>20</sup>

Inspired by light harvesting complexes in natural photosynthesis, numerous artificial light-harvesting architectures have been constructed to perform similar but simpler tasks such as sensitized luminescence or amplified quenching.<sup>21-25</sup> Among the artificial systems, MOFs provide a unique platform to study both short range and long range energy transfer phenomena due to the highly crystalline nature. In MOFs, the distance and orientation between chromophores can be precisely determined via single crystal X-ray crystallography, allowing theoretical prediction of electronic coupling and other interactions. The periodic alignment of chromophores also simplifies mathematical simulation and allows investigation of long range energy transfer, which is difficult to study in other supramolecular assemblies. The distances between chromophores can be tuned via crystal engineering, opening up the possibilities to construct a series of energy transfer systems that can provide mechanistic insights for energy transfer processes.

The porous structure of MOFs facilitates the diffusion of substrates and products through MOF channels,<sup>26</sup> making MOFs an ideal platform to incorporate catalytic centers. Indeed, an increasing number of reports have appeared in recent years using MOFs as single-site solid catalysts.<sup>27-29</sup> Catalytic active centers can be introduced into MOFs via incorporation into

either the metal nodes or the bridging ligands, and a combination of both leads to bi-functionalized MOFs for sequential multistep catalysis.<sup>30</sup> Importantly, MOFs also offer the opportunity to integrate both light-harvesting and catalytic components in a single solid platform to enable the conversion of solar energy to chemical energy via artificial photosynthesis. The hierarchical organization of MOFs thus has the potential to lead to multifunctional systems for solar energy utilization and to provide important insights into organizing multiple components in a spatially defined manner to elicit synergistic functions of multiple components.

Photo-sensitized organic reactions have received a renewed interest from the synthetic organic community in the past few years. The use of molecular dyes with absorption in the visible spectrum has enabled a range of organic transformations that do not proceed in thermally activated reactions or by direct photoexcitation of the organic substrates.<sup>31-36</sup> Most of these photocatalytic reactions invoke single electron transfer (SET) processes between dye molecules and substrates, with their efficiencies strongly dependent on excited state lifetimes of the dye molecules. The dye molecules used in these reactions typically have long-lived triplet excited states resulting from intersystem crossing upon singlet metal-to-ligand charge transfer (<sup>1</sup>MLCT) that is enabled by strong spin-orbit coupling of the second and third row transition metals. Consequently, precious metal complexes such as Ru(bpy)<sub>3</sub><sup>2+</sup> and Ir(ppy)<sub>3</sub> (bpy = 2,2'-bipyridine; ppy = 2-phenylpyridine) are required for photocatalytic organic transformations, which limits the utility of such processes for fine chemical synthesis owing to the scarcity, high cost, and high toxicity of precious metals. MOFs provide a possible solution to this problem. Porous and photosensitizing MOFs allow the diffusion of the organic substrates through the open channels to facilitate photosensitization, thereby efficiently promoting photocatalytic organic transformations. A variety of molecular dyes can be incorporated into MOFs to afford solid photocatalysts. The heterogeneous nature of MOF photocatalysis facilitates the recycling process and reduces the contamination of organic products by heavy metals.

Oxidative degradation of organic pollutants is another intensely investigated topic in photocatalysis with inorganic materials such as semiconductor nanoparticles, metal oxides and polyoxometalates. However, most inorganic materials only work well under UV irradiation, which limits their practical applications. MOFs serve as an alternative platform for developing efficient photocatalysts for degradation of organic pollutants because the broad choice of organic and metal-organic ligands in MOFs enables tuning of the absorption band and better utilization of the visible spectrum of sunlight.

In this review, we will summarize recent progress in using MOFs for artificial photosynthesis and photocatalysis. We will discuss light harvesting and energy transfer phenomena in MOFs, using MOFs as photocatalysts for promoting organic transformations and for organic pollutant degradation, and using MOFs in studying solar energy conversion reactions.

## Theoretical models for energy transfer in MOFs

The energy transfer process has attracted much interest from biologists, chemists, and physicists due to its crucial role in light harvesting for biological photosynthetic systems, molecular assemblies, and semiconductors. Fundamental understanding of energy transfer process in an extended system is also critical for other solar energy conversion schemes such as photovoltaics and photoelectrochemical cells. In molecular or supramolecular light harvesting architectures, photon energy is harvested by a dye molecule via photoexcitation and relayed to a “trap” state or a charge-separation center via energy transfer.

Different models have been developed to describe energy transfer processes in solid state materials and in supramolecular assemblies. In inorganic and organic semiconductors, energy transfer processes are usually described by the diffusion or transportation of localized (Frenkel) or delocalized (Wannier) excitons. Förster and Dexter energy transfer mechanisms<sup>37, 38</sup> are usually proposed for energy transfer in supramolecular assemblies given the weak coupling between chromophores. As interactions between chromophores are expected to be weak in MOFs due to the long distance between them, Förster and Dexter mechanisms provide more convenient descriptions for MOFs. At this weak coupling limit, Förster energy transfer model presumes that only the dipole-dipole term of Coulomb interaction is important and has to be taken into account, whereas Dexter mechanism introduces an “exchange” term which can be schematically considered as exchanging electrons between a donor and an acceptor (Figure 2).

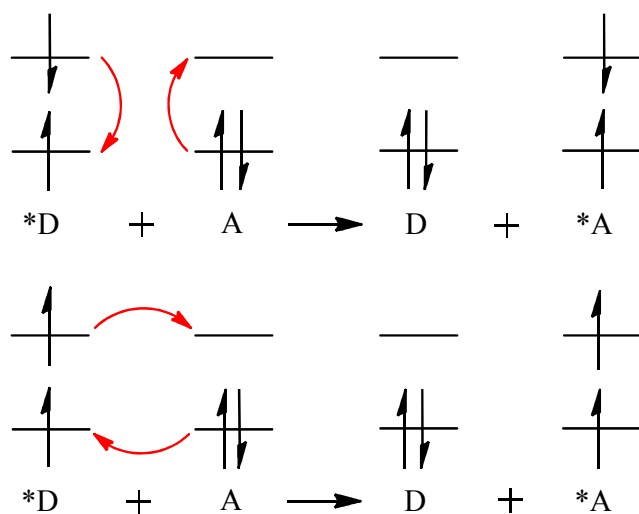


**Figure 2.** Schematic representations of Förster (top) and Dexter (bottom) energy transfer mechanisms.

In MOFs as well as in other supramolecular and polymeric systems, the weak coupling criterion is shown to be valid. Energy transfer rates predicted from both Förster and Dexter terms decrease as the donor-acceptor distance increases, yet following different dependencies on distances. The Förster

energy transfer rate is proportional to inverse sixth-power of the donor-acceptor distance

$$k_{ET} = \frac{1}{\tau_f} \left( \frac{R_0}{R} \right)^6$$

while the Dexter energy transfer rate exhibits exponential decay<sup>39</sup>

$$k_{ET} = \left( \frac{2\pi}{\hbar} \right)^2 K^2 \exp\left(-\frac{2R}{L}\right) \int f_D(\nu) f_A(\nu) d\nu$$

Thus, Förster mechanism dominates long distance energy transfer processes when both pathways are symmetry allowed, while Dexter mechanism is only important within a short range. However, Förster mechanism requires spin state conservation of both donor and acceptor wave functions. In the cases of triplet-triplet energy transfer, Förster mechanism is spin forbidden and Dexter mechanism will play an important role in depicting the energy transfer process.

## Rational design of photocatalytic MOFs

MOFs have been proposed as potential photocatalysts since late 1990's and early 2000's. Early research on MOF photocatalysis stood on the belief that MOFs were analogous to inorganic semiconductors given the extended structure formed by linking bridging ligands and metal connecting nodes in MOFs. The concept of MOFs as a class of semiconducting material was proposed because many MOFs exhibit a broad UV-vis absorption with an edge falling into the range of typical semiconductor band gap values. However, such an absorption band can also be assigned to a localized ligand-to-metal charge transfer (LMCT) or metal-to-ligand charge transfer (MLCT) transition or a  $\pi$ - $\pi^*$  transition of the aromatic ligand. The broad band nature of MOF absorption can be attributed to inhomogeneous broadening, which is not uncommon in solid state samples. The optical absorption data thus cannot be taken as strong evidence to support the description of MOFs as semiconductors.

The insulating nature of MOFs is further suggested from theoretical studies. Poor overlap between frontier orbitals indicates that the electronic states in MOFs are more localized than delocalized.<sup>40</sup> Calculation on a typical MOF, **MOF-5**, suggests no appreciable band dispersion in its electronic structure.<sup>41</sup> Thus, charge separation over a long distance will not be observed upon excitation, which is consistent with the low charge mobility of most MOFs.

Similar to the case of MOF catalysis, we can define MOF photocatalysis in two classes: “opportunistic” photocatalysis and designer photocatalysis.<sup>28</sup> Many photocatalytic MOFs reported to date belong to the first class, taking advantage of the broad absorption of LMCT or ligand  $\pi$ - $\pi^*$  bands. There exist several drawbacks for this scheme. The relative energies of HOMO and LUMO orbitals cannot be readily tuned, and the lifetimes of the excited states can be too short to perform

interesting chemistry. These MOFs usually exhibit low efficiency in the sense of photon energy utilization, and are typically used for oxidative dye degradation reactions which tend to have large thermodynamic driving forces and small kinetic barriers.

Bridging ligands based on well-known organic and metal-organic chromophores have also been used as building blocks to construct photocatalytic MOFs. With better knowledge about the photophysical properties of the chromophoric building blocks, MOFs photocatalysts with much higher efficiency can be designed to promote more sophisticated, difficult-to-catalyze, and useful reactions. More advanced designs use more than one functional component in the framework. For example, metal nanoparticles were incorporated as a co-catalyst for hydrogen evolution either through diffusion<sup>42, 43</sup> or in situ synthesis;<sup>44</sup> chiral organocatalysts were also introduced to perform asymmetric photocatalysis.<sup>45</sup> Multi-component MOFs provide significant advantages in performing these photocatalytic reactions as the proximity of different components in the MOFs synergistically interact to provide enhanced catalytic performances.

### Energy transfer and light harvesting in MOFs

Ligand-sensitized luminescence, one form of energy transfer, has been extensively studied in MOFs built from lanthanide metals.<sup>46-57</sup> In these MOFs, the organic ligands serve as antenna to sensitize lanthanide metal nodes, whose *f-f* transitions typically have small extinction coefficients. As a result, strong characteristic *f-f* emission peaks can be observed upon excitation at the ligand absorption band. Of particular interest are the organic ligands with low-lying triplet excited states, for in these cases energy transfer to the lanthanide resonance levels is spin allowed.<sup>53, 58, 59</sup> These energy transfer processes are usually proposed to follow a Förster mechanism.

Efficient energy transfer has also been observed between adjacent donor-acceptor ligand pairs or between ligand and guest molecules in MOFs.<sup>47, 60-64</sup> In 2009, Loh and coworkers reported the efficient energy transfer in a 1-D nanoscale coordination polymer between  $\pi$ -conjugated chromophores.<sup>60</sup> Hupp and coworkers encapsulated CdSe/ZnS core/shell quantum dots into the MOF channel, and studied the energy transfer from the quantum dots to the porphyrin-derived ligands of the framework. The energy transfer efficiency can be tuned upon varying the quantum dot sizes to change their spectra.<sup>63</sup>

Recently, MOFs were utilized to mimic the natural light-harvesting complexes and to study energy transfer behaviors over long distances. One of the first examples was reported by Lin, Meyer and coworkers in 2010.<sup>65</sup> A phosphorescent MOF  $\text{Zn}(\text{L}_1\text{-Ru})\cdot 2\text{DMF}\cdot 4\text{H}_2\text{O}$  (**1**) was synthesized from  $\text{Ru}(\text{bpy})(4,4'\text{-dcbpy})_2[\text{PF}_6]_2$  bridging ligand ( $\text{H}_2\text{L}_1\text{-Ru}[\text{PF}_6]_2$ , 4,4'-dcbpy = 2,2'-bipyridine-4,4'-dicarboxylic acid) and  $\text{Zn}^{2+}$  connecting nodes. **1** can be excited to the <sup>1</sup>MLCT state of the **L<sub>1</sub>-Ru** bridging ligand and exhibit phosphorescence (following intersystem crossing to the <sup>3</sup>MLCT excited state due to large spin-orbit coupling of Ru(II) centers) with a lifetime

approaching several hundreds of nanoseconds. When the osmium analog of the bridging ligand, **L<sub>1</sub>-Os**, was doped into the framework, the <sup>3</sup>MLCT excited states of **L<sub>1</sub>-Ru** were readily quenched due to energy migration to the osmium trap sites. Time-resolved emission studies showed that the lifetimes of Ru(II) excited states decreased as the doping level of Os(II) increased. A growth of Os(II) emission provided strong evidence for Ru-to-Ru excited state migration and Ru-to-Os energy transfer in osmium-doped **1** (Figure 3).

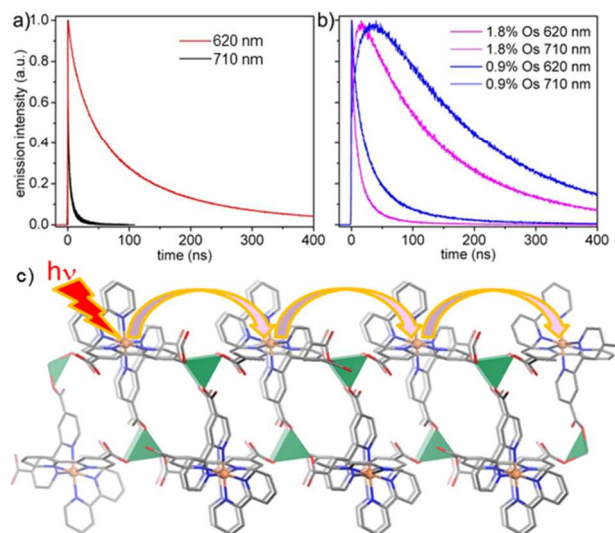


**Figure 3.** a) Transient emission decay profiles for **1** and its osmium analog, **1-Os**, monitored at 620 nm and 710 nm, respectively, following two-photon excitation at 850 nm. b) Transients for 1.4 and 2.6 mol% Os-doped **1** at 620 nm and 710 nm with emission at 620 nm dominated by  $\text{Ru}^{\text{II}*}$  and at 710 nm by  $\text{Os}^{\text{II}*}$ . c) Schematic depicting the hopping of the  $\text{Ru}(\text{II})^*\text{-bpy}$  excited states in these isomorphous MOFs. Reprinted with permission from reference <sup>65</sup>. Copyright 2010 American Chemical Society.

Since Förster mechanism is spin-forbidden in this triplet-triplet energy transfer process, the energy transfer in **1** was initially proposed as a site-by-site hopping following Dexter mechanism. A one-dimensional diffusive (random walk) model was used to describe the energy transfer map across the framework. However, the fitted energy transfer rates are faster than those predicted from a Dexter model, suggesting some cooperative or long range effects.<sup>66</sup>

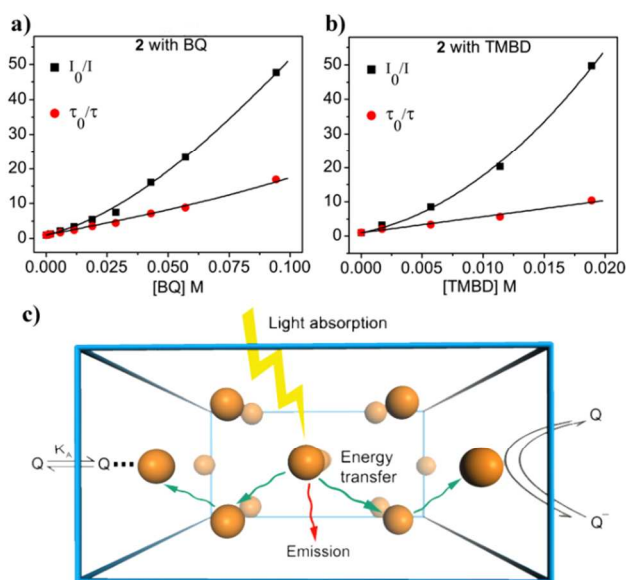


**Figure 4.** a,b) Steady-state (black) and time-resolved (red) Stern-Volmer quenching analysis of **2** with BQ (a) or TMBD (b). c) Schematic showing the light-harvesting process in MOF microcrystals as a result of a rapid energy migration over several hundred nanometers followed by efficient electron transfer quenching at the MOF/solution interface. Reprinted with permission from reference<sup>67</sup>. Copyright 2011 American Chemical Society.

Efficient light-harvesting as a result of rapid energy migration in **1** and another MOF,  $\text{Zn}(\text{H}_2\text{L}_2) \cdot 3\text{H}_2\text{O}$  (**2**,  $\text{H}_2\text{L}_2 = \text{Ru}(4,4'\text{-dcbpy})_2(\text{CN})_2$ ), which is built from a similar ruthenium-based bridging ligand, was probed by luminescence quenching studies using an oxidative quencher (1,4-benzoquinone) or a reductive quencher (N, N, N', N'-tetramethylbenzidine). The quenching process was proposed to take place at the MOF/solution interface as the MOF channels are too small to allow quencher molecules to diffuse in. The quenching behavior showed different quencher concentration dependence for intensity and lifetime measurements. When the lifetime followed Stern-Volmer equation, the luminescence intensity exhibited a positive deviation (Figure 4). Thus, the quenching data were fitted with a model considering both static (pre-association) and dynamic (diffusion) quenching processes:

$$\frac{I_0}{I} = \left[ (1 - \gamma) + \gamma F_{SQ} \frac{k_{\text{Ru}^*}}{k_{\text{Ru}^*} + k_S} + \gamma (1 - F_{SQ}) \frac{k_{\text{Ru}^*}}{k_{\text{Ru}^*} + k_D [Q]} \right]^{-1}$$

$$\frac{\tau_0}{\tau} = \frac{1}{k_{\text{Ru}^*} \langle \tau \rangle}$$

where  $k_S$  and  $k_D$  are rate constants for static and dynamic quenching, respectively.  $\gamma$  is the excited states migrated to the MOF/solution interface, which was found to be nearly 1 upon fitting. These results indicated that the excited states rapidly migrate over hundreds of nanometers to the MOF/solution interface with a near unity efficiency.<sup>67</sup> A follow-up study

showed that **2** exhibited a 7000-fold enhancement of Stern-Volmer quenching constant compared to the moiety complex  $\text{Ru}(\text{bpy})_2(\text{CN})_2$  with methylene blue as the quencher.<sup>68</sup> These phosphorescent MOFs thus provide a promising platform to develop highly sensitive and selective sensors.

Rapid energy transfer processes were also reported in porphyrin-based MOFs. Hupp and coworkers studied the energy transfer phenomena in two MOFs,  $\text{Zn}_2(\text{TCPB})(\text{F-ZnP})$  (**F-MOF**,  $\text{H}_4\text{TCPB} = 1,2,4,5\text{-tetrakis}(4\text{-carboxyphenyl})\text{benzene}$ ,  $\text{F-ZnP} = [5,15\text{-di}(4\text{-pyridyl})\text{-}10,20\text{-bis}(\text{pentafluorophenyl})\text{porphyrinato}] \text{zinc}(\text{II})$ ) and  $\text{Zn}_2(\text{TCPB})(\text{DA-ZnP})$  (**DA-MOF**,  $\text{DA-ZnP} = [5,15\text{-bis}[(4\text{-pyridyl})\text{ethynyl}]\text{-}10,20\text{-diphenylporphyrinato}] \text{zinc}(\text{II})$ ), with porphyrin-derived ligands.<sup>69</sup> Both MOFs adopt pillar-layer structures with the porphyrin-derived ligands sitting at the pillar positions and aligning in rectangle geometry (Figure 5). Enhanced quenching was observed with pyridyl-ferrocene (FcPy) as a pre-associated quencher. In both MOFs, the fluorescence quenching follows a modified Stern-Volmer equation:

$$\frac{I_0 - I_s}{I - I_s} = 1 + K_{SV}[Q]$$

where  $I_0$ ,  $I$ , and  $I_s$  represent fluorescence intensities at zero quencher doping level, a particular quencher doping level, and saturated quencher doping level, respectively. The saturated quenching phenomenon is consistent with a pre-association quenching process.

Theoretical studies suggested that energy transfer between porphyrin chromophores is anisotropic with the intra-layer rates (pathways AB, AC, and AD in Figure 5) faster than inter-layer rates (pathway AE) in **F-MOF**. However, the inter-layer energy transfer is not negligible in **DA-MOF** despite a longer chromophore distance.

A one-dimensional model was used to estimate the total hopping steps of the excited state within its lifetime. However, this oversimplified model underestimated the ability of a trap site to quench migrating excited states due to the reduced dimension, potentially leading to an overestimation of energy transfer rates. This much more significant amplified quenching effect in a three-dimensional network compared to a one-dimensional system was also reported by Lin, Meyer and coworkers.<sup>70</sup>

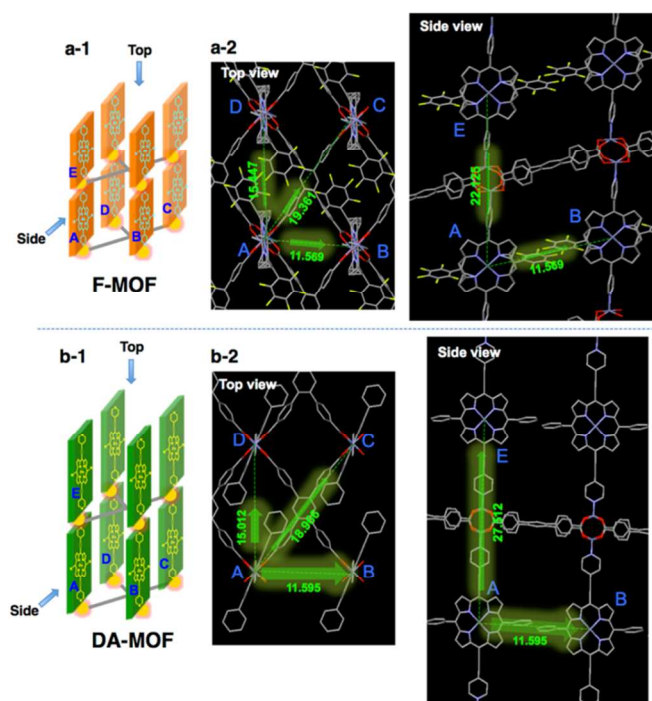


**Figure 5.** Schematic figures showing the structure and distances between porphyrin chromophores in **F-MOF** (a) and **DA-MOF** (b). Reprinted with permission from reference <sup>69</sup>. Copyright 2013 American Chemical Society.

Hupp and coworkers also carried out a follow-up study fabricating thin films of **DA-MOF** in a layer-by-layer manner.<sup>71</sup> The resulting MOF thin films were then decorated by a second squaraine dye **S1** (Figure 6a)<sup>72</sup> at the outermost layer as an acceptor to probe energy transfer. Photophysical studies showed that the porphyrin chromophores were completely quenched by the second dye in a 50-cycle film, suggesting very efficient energy transfer in this MOF (Figure 6).

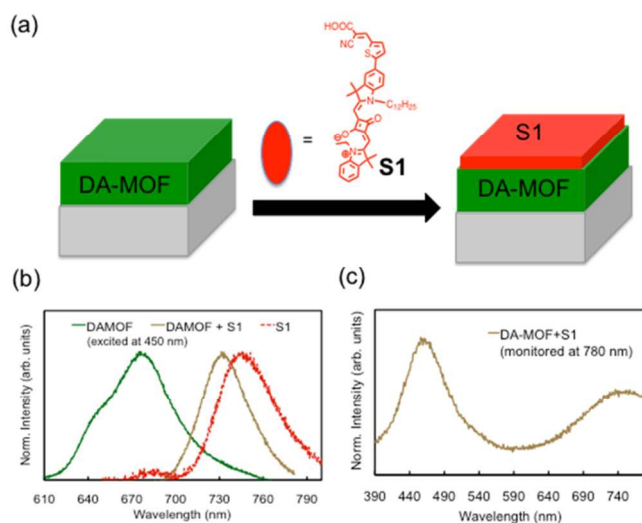


**Figure 6.** (a) Preparation of **S1**-decorated **DA-MOF** film. (b) Comparison of emission profiles of **DA-MOF** (green), **S1** (red), and **DA-MOF** sensitized **S1** (brown) upon excitation at 450 nm. (c) Excitation profile of the **DA-MOF+S1** film

monitored at 780 nm, where the emission from **DA-MOF** is negligible. Reprinted with permission from reference <sup>71</sup>. Copyright 2013 American Chemical Society.

Energy transfer between different lanthanide ions has also been investigated. Reddy and coworkers studied the energy transfer from a  $Tb^{3+}$  center to an  $Eu^{3+}$  center in a mixed-lanthanide MOF  $[Eu_{0.5}Tb_{0.5}L_3(H_2O)_2]_n$  [**3**,  $L = 4$ -(dipyridin-2-yl)aminobenzoate].<sup>73</sup> The energy transfer efficiency was determined to be 86% based on lifetime measurements. A Förster mechanism was proposed for the energy transfer process.

### MOFs for photocatalytic oxidative degradation of organic molecules

Photocatalytic degradation of organic pollutants is one of the intensely studied topics in environmental science. Quite a number of MOFs have been investigated as photosensitizers for decomposing organic dye molecules that are used as surrogates for organic pollutants. Simple MOFs such as **MOF-5**,<sup>74</sup> **MIL-100(Fe)**<sup>75</sup> or **MIL-53(Fe)**<sup>76</sup> can be excited under UV or visible irradiations to LMCT states, which will sensitize oxygen and show catalytic activity towards oxidative degradation of organic molecules.<sup>77-80</sup> In 2007, Garcia and coworkers reported oxidative degradation of substituted phenols with **MOF-5** under UV light. A reverse size selectivity was observed for phenol and 2,6-di-*tert*-butylphenol, while the bulkier substrate exhibited a higher degradation rate. This reverse selectivity suggests that the degradation process likely takes place on the external surface of the MOF.<sup>78</sup> The authors however did not rule out the possibility that the observed reactivity trend is due to the fact that electron-rich 2,6-di-*tert*-butylphenol is easier to oxidize than phenol.

Organic dyes such as methylene blue, rhodamine B, or methyl orange are more widely used as probes to examine photocatalytic activities of MOFs, for it is convenient to monitor the dye degradation using UV-vis absorption spectroscopy.<sup>81-91</sup> A titanium(IV) based MOF,  $Ti_2(H_4dhdcc)_2(H_2dhdcc)$  (**NTU-9**,  $H_4dhdcc = 2,5$ -dihydroxyterephthalic acid), was reported recently as an active photocatalyst for dye degradation.<sup>92</sup> In **NTU-9**, the mononuclear titanium(IV) centres are connected through 2,5-dihydroxyterephthalate ligand to form a 2-D sheet. Due to the strong LMCT absorption, **NTU-9** shows deep red colour with an absorption band extending to 750 nm. **NTU-9** exhibited excellent photocatalytic activity towards dye degradation. Rhodamine B and methylene blue were completely degraded upon 80 min and 20 min of visible light irradiation, respectively.

Although many MOFs have been reported to exhibit good to excellent performance in dye degradation compared to conventional standards such as  $TiO_2$ , not much effort has been devoted to kinetic or mechanistic studies for those systems. One of the several kinetic studies was carried out by Li and coworkers in 2012. They used terephthalic acid as a probe molecule to detect the formation and existence of hydroxyl

radicals in photocatalytic dye degradation reactions.<sup>87</sup> They used the ligands 1,2,4,5-benzenetetracarboxylic acid ( $H_4\text{btcc}$ ) and 4,4'-bis(1-imidazolyl)biphenyl ( $\text{bimb}$ ) to synthesize a family of MOFs with different metal ions. Three of them,  $[\text{Co}(\text{btcc})_{0.5}(\text{bimb})]_n$  (**4**),  $[\text{Ni}(\text{btcc})_{0.5}(\text{bimb})(\text{H}_2\text{O})]_n$  (**5**), and  $[\text{Cd}(\text{btcc})_{0.5}(\text{bimb})_{0.5}]_n$  (**6**), exhibited good performance for oxidative degradation of the organic dye X3B. The photogenerated hydroxyl radical was scavenged by terephthalic acid to form a luminescent product 2-hydroxyterephthalic acid. No photoluminescence (PL) intensity increase was observed in absence of the MOFs, while the PL intensity of 2-hydroxyterephthalic acid showed linear relationship with time at the presence of visible light and MOF catalysts (Figure 7). The zeroth-order kinetics indicated that the generation of hydroxyl radicals takes place at the MOF/solution surface via photochemical processes.

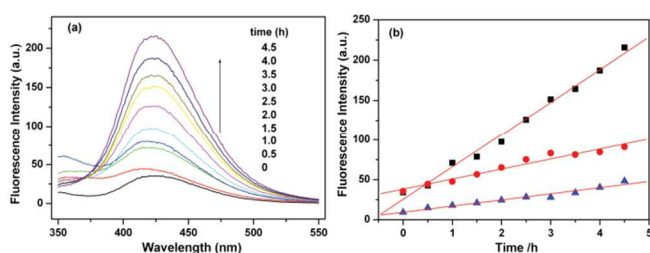


**Figure 7.** (a) PL spectral changes observed during illumination of **6** in a  $5 \times 10^{-4}$  M basic solution of terephthalic acid (excitation at 315 nm). (b) Comparison of the induced PL intensity at 425 nm for MOFs **4** (red), **5** (blue), and **6** (black). Reprinted with permission from reference <sup>87</sup>. Copyright 2012 American Chemical Society.

## MOFs for organic photocatalysis

Compared to the intensively studied dye degradation reactions, much less effort has been devoted to photocatalytic transformations, which require better control of excited state properties. Lin and coworkers first incorporated metal-organic dyes such as  $\text{Ru}(\text{bpy})_3^{2+}$  or  $\text{Ir}(\text{ppy})_2(\text{bpy})^+$  into UiO-type MOFs and obtained solid state photocatalysts.<sup>93</sup> Aza-Henry reactions, oxidative coupling of amines and oxidation of sulfides were investigated as model reactions to demonstrate the photocatalytic activities of these MOFs. The resulting MOFs showed slightly lower activity compared to homogeneous controls, yet exhibited excellent reusability as no decrease of catalytic activity was observed. However, as size-selectivity was not observed in photocatalysis, it was suggested that these reactions could be mediated by photochemically generated singlet oxygen.

Wu and coworkers reported a tin-porphyrin MOF  $[\text{Zn}_2(\text{H}_2\text{O})_4\text{Sn}^{\text{IV}}(\text{TPyP})(\text{HCOO})_2] \cdot 4\text{NO}_3 \cdot \text{DMF} \cdot 4\text{H}_2\text{O}$  (**7**,  $\text{Sn}^{\text{IV}}\text{TPyP}$  = 5,10,15,20-tetra(4-pyridyl)-tin(IV)-porphyrin) as a photocatalyst for oxidation of sulfides to sulfoxides.<sup>94</sup> **7** exhibited better selectivity towards sulfoxides than the homogeneous control,  $\text{Sn}^{\text{IV}}(\text{OH})_2\text{TPyP}$ . The MOF also catalyzed photochemical oxidation of 1,5-dihydroxynaphthalene to 5-hydroxynaphthalene-1,4-dione.

Combination of a photosensitizer and an asymmetric catalyst in the same MOF can lead to stereoselective photocatalysis. Duan and coworkers reported in 2012 a pair of MOF enantiomers as asymmetric photocatalysts.<sup>45</sup> The MOFs were constructed from photoactive tris(4-carboxyphenyl)amine ( $H_3\text{TCA}$ ) ligands and  $\text{Zn}^{2+}$  metal ions with L- or D-N-t-butoxycarbonyl-2-(imidazole)-1-pyrrolidine (L- or D-**BCIP**) as a chiral adductive. Framework chirality was confirmed via single crystal crystallography and circular dichroism (CD) spectroscopy. The protected chiral amine not only serves as a template for the synthesis of the chiral MOF, but also shows catalytic activity upon thermal deprotection (Figure 8). The deprotected MOFs,  $\text{Zn}_2(\mu\text{-OH})(\text{OH}_2)(\text{TCA})(\text{L-PYI})$  (**Zn-PYI1**, L-PYI = L-pyrrolidine-2-ylimidazole) and its mirror image **Zn-PYI2**, were used as heterogeneous photocatalysts for asymmetric  $\alpha$ -alkylation of aliphatic aldehydes. Remarkably high enantioselectivities were achieved, and different hands of MOFs gave opposite selectivities.

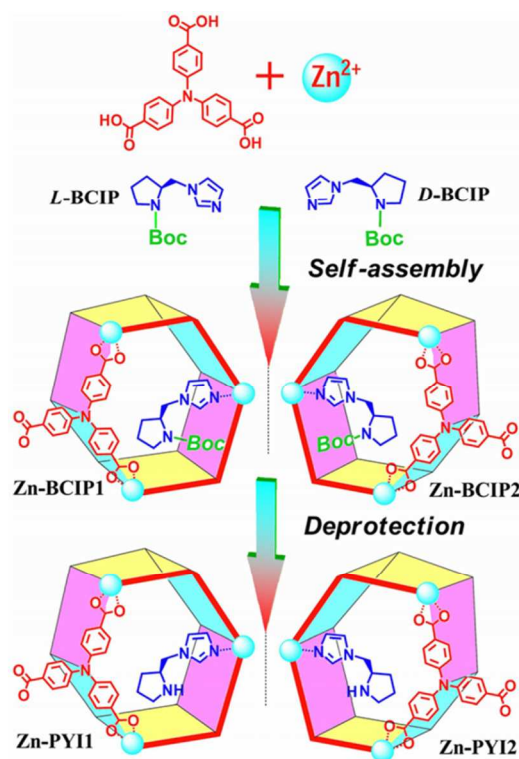


**Figure 8.** Schematic representation of mirror image structures of **Zn-BCIP1** and **Zn-BCIP2** and their deprotected forms **Zn-PYI1** or **Zn-PYI2**. Reprinted with permission from reference <sup>45</sup>. Copyright 2012 American Chemical Society.

The two MOFs were studied thoroughly to demonstrate the catalytic activity and selectivity. First, substrates of the reaction, the aldehyde and ethyl bromomalonate, can be adsorbed into the MOF channel. Bromomalonate was also shown to quench the luminescence of the photoactive ligand tris(4-carboxyphenyl)amine. Second, size selectivity was observed when different aldehydes were used. These experiments proved that the catalysis took place in the channel of the MOFs, not only on the external surface. Catalysis experiments were also performed using achiral MOFs  $\text{Ho}_4(\mu_3-$

$\text{O}_2(\mu_3\text{-OH})_2(\text{H}_2\text{O})_8(\text{TCA})_2$  or  $\text{Zn}_4\text{O}(\text{TCA})_2$  (**MOF-150**)<sup>95,96</sup> as the photosensitizer, which bear the same photoactive moiety, with the same chiral adduct. Although the chiral adduct can also be adsorbed, much lower enantiomeric excess (ee) values were obtained in catalysis. The results indicated that framework chirality also plays an important role in the asymmetric photocatalysis, and combination of both photoactive and asymmetric components in the same framework is essential to achieve enantioselectivity.

### MOFs for photocatalytic hydrogen evolution and CO<sub>2</sub> reduction

Photo-driven water splitting or CO<sub>2</sub> reduction is one of the most promising scenarios for solar energy conversion. Various molecular compounds, semiconductors and hybrid materials have been developed in the past few decades for water splitting and CO<sub>2</sub> reduction reactions. As the LMCT and ligand  $\pi\text{-}\pi^*$  excitation of MOFs fall into UV and the blue end of visible regions, MOFs have been proposed to exhibit similar photocatalytic activities as semiconductors, which have similar band gap values. Simple MOFs such as **UiO-66**<sup>97</sup> have been tested as a photocatalyst for hydrogen evolution. **UiO-66** showed catalytic activity for hydrogen evolution in a methanol/water mix solution, and enhanced activity was observed when platinum nanoparticles were added as a co-catalyst.<sup>42</sup> Introduction of a pending amino group to the MOF backbone resulted in an intense absorption band between 300–400 nm and slightly increased the catalytic activity. The amino-functionalized MOF, **NH<sub>2</sub>-UiO-66**, was also found to exhibit modest catalytic activity towards CO<sub>2</sub> reduction recently.<sup>98</sup>

Using a similar strategy, Li and coworkers reported in 2012 photocatalytic CO<sub>2</sub> reduction catalyzed by **NH<sub>2</sub>-MIL-125(Ti)**, a MOF constructed from  $\text{Ti}_8\text{O}_8(\text{OH})_4(\text{O}_2\text{CR})_{12}$  clusters and 2-aminoterephthalic acid bridging ligands (Figure 9).<sup>99</sup> **NH<sub>2</sub>-MIL-125(Ti)** exhibits a visible absorption band extending to 550 nm. Photocatalytic CO<sub>2</sub> reduction was performed under visible light with triethanolamine (TEOA) as the sacrificial electron donor in acetonitrile solution. Formate was detected as the reducing product. A modest TON of 0.03 per Ti was achieved.

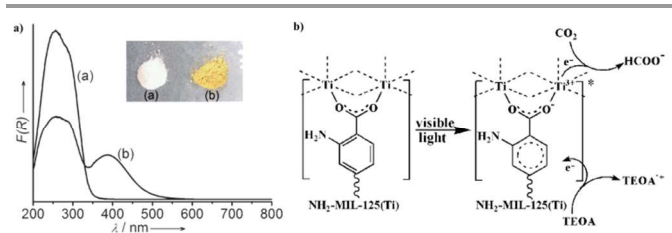


**Figure 9.** (a) Absorption spectra of MIL-125(Ti) (line a) and NH<sub>2</sub>-MIL-125(Ti) (line b). (b) Proposed mechanism for the photocatalytic CO<sub>2</sub> reduction. Reprinted with permission from reference<sup>99</sup>. Copyright 2012 Wiley-VCH.

Although photo-mediated reactions can be achieved with these simple MOFs, the activities are very low and most of the studied systems are not catalytic (in a strict sense) with a TON of less than 1. This low photocatalytic activity is probably due

to the absence of vacant sites for substrate activation and inefficient electron transfer between the MOF and the substrate. To enhance their performances, several MOFs have been designed and used as either photosensitizers or catalysts in multi-component photocatalytic systems. In 2009, Mori and coworkers reported a MOF  $[\text{Ru}_2(\text{p-BDC})_2]_n$  as a catalyst for a photochemically driven hydrogen evolution reaction.<sup>100</sup> The MOF was constructed from  $\text{Ru}_2(\text{O}_2\text{CR})_4$  paddle-wheel secondary building units (SBUs) and linear BDC linkers, leading to a two-dimensional structure with one-dimensional channels running perpendicular to the layers. The SBUs are catalytic active for proton reduction with  $\text{Ru}(\text{bpy})_3^{2+}$  as the photosensitizer, methyl viologen ( $\text{MV}^{2+}$ ) as the electron relay, and  $\text{Na}_2\text{EDTA}$  as the sacrificial electron donor. All the four components were found to be critical for hydrogen generation.

Rosseinsky and coworkers used a water stable porphyrin MOF  $\text{Al}_2(\text{OH})_2(\text{TCPP})\cdot 3\text{DMF}\cdot 2\text{H}_2\text{O}$  ( $\text{H}_4\text{TCPP}$  = *meso*-tetra(4-carboxyphenyl)porphyrin) as the photosensitizer for photocatalytic proton reduction with platinum nanoparticles as a co-catalyst and  $\text{Na}_2\text{EDTA}$  as the sacrificial electron donor.<sup>43</sup> An approximate TON of 0.7H<sub>2</sub>/porphyrin was achieved over 6 hours, however, when  $\text{MV}^{2+}$  was introduced to the system as an electron relay, the catalytic activity decreased by one order of magnitude. The author suggested that slow diffusion of  $\text{MV}^{2+}$  through MOF channels leads to inefficient electron transfer and low activity.

Lin and coworkers reported in 2011 the synthesis of a MOF photocatalyst  $\text{Zr}_6(\mu_3\text{-O})_4(\mu_3\text{-OH})_4(\text{bpdc})_{5.83}(\text{L}_8)_{0.17}$  (**8**, bpdc = 5,5'-biphenyldicarboxylate;  $\text{H}_2\text{L}_8$  =  $\text{Re}(\text{CO})_3(5,5'\text{-dcbpy})\text{Cl}$ ) by doping  $[\text{Re}(\text{CO})_3(5,5'\text{-dcbpy})\text{Cl}]$  into a **UiO-67** framework.<sup>93</sup>  $\text{Re}(\text{bpy})(\text{CO})_3\text{X}$  has been extensively studied as molecular CO<sub>2</sub> reduction catalysts in homogeneous systems. **8** showed the same powder X-ray diffraction (PXRD) pattern as **UiO-67** due to the matching lengths of  $[\text{Re}(\text{CO})_3(5,5'\text{-dcbpy})\text{Cl}]$  and 4,4'-biphenyldicarboxylic acid. **8** catalyzed highly selective photocatalytic CO<sub>2</sub> reduction towards CO in acetonitrile solution with triethylamine as a sacrificial reducing agent. A TON of 10.9 was achieved in 12 hours, which is almost three times higher than that of the homogeneous complex. The higher activity was believed to result from site isolation of catalytic centers, which blocks bimolecular catalyst decomposition pathways. However, the recovered solid was inactive for CO generation. Spectroscopic studies showed the loss of CO stretching vibrations and the MLCT absorption band, indicating that the rhenium-carbonyl moieties detached from the MOF backbone during the catalytic cycle.

Ott and coworkers recently reported the incorporation of a  $[\text{FeFe}]$ -hydrogenase analog,  $\text{Fe}_2(\text{dcbdt})(\text{CO})_6$ , into **UiO-66** framework via post-synthetic exchange method.<sup>101</sup> EDX studies indicated that ~14% of the bridging ligand was exchanged to  $\text{Fe}_2(\text{dcbdt})(\text{CO})_6$ . The resulting MOF solid was three times more active than the corresponding ligand towards photochemical proton reduction with  $\text{Ru}(\text{bpy})_3^{2+}$  as the photosensitizer and ascorbic acid as the sacrificial electron donor. The activity enhancement was attributed to stabilization of the catalyst in the framework and inhibition of

nonproductive charge recombination. The stability of the UiO framework under the catalytic conditions was however not demonstrated in this work.

Recently, Wang and coworkers reported the photocatalytic activity of a cobalt-based zeolitic imidazolate framework  $\text{Co}(\text{benzimidazole})_2$  (**Co-ZIF-9**), which was first reported in 2006.<sup>102, 103</sup> **Co-ZIF-9** showed photocatalytic activities towards proton and  $\text{CO}_2$  reduction in the presence of  $\text{Ru}(\text{bpy})_3^{2+}$  photosensitizer, TEOA sacrificial reducing agent and visible light. A mixture solution of  $\text{Co}^{2+}$  and benzimidazole ligand also showed some catalytic activity, but lower than that of **Co-ZIF-9**. However, the selectivity of  $\text{CO}_2$  reduction against proton reduction is moderate. Control experiments indicated that the efficiency for proton reduction increased greatly in the presence of  $\text{CO}_2$ , but it remains unclear whether it is due to pH difference or  $\text{CO}_2$  plays a role in the hydrogen evolution catalytic cycle.

For most MOFs, a second component, either a photosensitizer or a co-catalyst, is needed to get significant TONs for proton or  $\text{CO}_2$  reduction. In these cases, slow mass transport through MOF channels and inefficient electron transfer between MOF and the homogeneous component will greatly affect the performance and decrease the activity. Better designs are thus needed to integrate different components in a single solid to obtain a more active catalyst. In 2012, Lin and coworkers reported a MOF-based assembly consisting of phosphorescent MOF backbone and platinum nanoparticles for hydrogen evolution.<sup>44</sup> They used iridium(III) based molecular photosensitizers bis(4-phenyl-2-pyridine)(5,5'-dicarboxylate)-2,2'-bipyridine-iridium(III) chloride (**L<sub>9</sub>**) or bis(4-phenyl-2-pyridine)(5,5'-di(4-phenylcarboxylate)-2,2'-bipyridine)-iridium(III) chloride (**L<sub>10</sub>**) as the bridging ligand to synthesize UiO-type MOFs  $\text{Zr}_6(\mu_3\text{-O})_4(\mu_3\text{-OH})_4(\text{bpdc})_{5.94}$  (**L<sub>9</sub>**)<sub>0.06</sub> (**9**) and  $\text{Zr}_6(\mu_3\text{-O})_4(\mu_3\text{-OH})_4(\text{L}_{10})_6$  (**10**) (Figure 10). Upon irradiation, the excited photosensitizers trigger the photoreduction of a platinum(II) precursor to selectively deposit platinum nanoparticles in MOF channels. Both nanoparticle@MOF assemblies **Pt@9** and **Pt@10** showed catalytic activities for proton reduction reaction with triethylamine as the sacrificial reductant. TONs observed for **Pt@9** (TON=3400) and **Pt@10** (TON=7000) were 1.5 and 5 times as high as that of the homogeneous control, respectively. The close proximity of the photosensitizer (iridium complex molecules) and the catalyst (platinum nanoparticles) is believed to facilitate electron transfer between the two and enhance the catalytic performance. This work provides an interesting strategy to construct MOF-based hierarchical assemblies for solar energy conversion reactions.

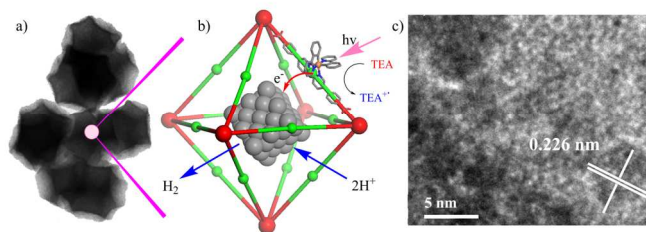


**Figure 10.** (a) TEM images of **Pt@9**. (b) The synergistic photocatalytic hydrogen generation process via photoinjection of electron from the light-harvesting MOF on to the Pt NPs. (c) HRTEM images of a powdery sample of **Pt@10**. The lattice fringes of the Pt particles are shown with d-spacing matching that of the Pt(111) plane. Reprinted with permission from reference <sup>44</sup>. Copyright 2012 American Chemical Society.

## MOFs for water oxidation

With quite a number of MOFs and MOF-based assemblies have been used as photocatalysts for hydrogen evolution, fewer MOF examples have been reported for the other half reaction of water splitting, namely water oxidation. This is probably due to the instability of most MOFs under water oxidation conditions (aqueous buffer solution, strong oxidant, etc.). The first work using MOF as a water oxidation catalyst was performed by Lin and coworkers in 2011.<sup>93</sup> Three iridium-based water oxidation catalyst,  $[\text{Cp}^*\text{Ir}^{\text{III}}(\text{dcppy})\text{Cl}]$ ,  $[\text{Cp}^*\text{Ir}^{\text{III}}(\text{dcbpy})\text{Cl}]\text{Cl}$ , and  $[\text{Ir}^{\text{III}}(\text{dcppy})_2(\text{H}_2\text{O})_2]\text{OTf}$ , (dcbpy = 2,2'-bipyridine-5,5'-dicarboxylic acid; dcbpy = 2,2'-bipyridine-5,5'-dicarboxylic acid) were doped into the **UiO-67** framework and the resulting MOFs showed catalytic activity towards cerium(IV) driven water oxidation. However, all three MOFs showed much lower activity compared to their homogeneous counterparts. The authors believed that catalytic water oxidation only takes place near the external surface of the MOFs since cerium(IV) cannot enter the MOF channels due to the small MOF open channel sizes.

To enhance water oxidation activities, Lin and coworkers prepared catalytic active MOFs with larger channels using an Ir-based longer bridging ligand. In 2012, they reported two MOFs,  $\text{Zr}_6(\mu_3\text{-O})_4(\mu_3\text{-OH})_4\{[(\text{bpy-dc})\text{IrCp}^*\text{Cl}]\text{Cl}\}_6$  (**11**,  $\text{H}_2\text{bpy-dc}$  = 5,5'-bis(4-carboxyphenyl)-2,2'-bipyridine) and  $\text{Zr}_6(\mu_3\text{-O})_4(\mu_3\text{-OH})_4[(\text{ppy-dc})\text{IrCp}^*\text{Cl}]_6$  (**12**,  $\text{H}_2\text{ppy-dc}$  = 2-(4'-carboxyphenyl)phenyl-5-(4-carboxyphenyl)pyridine), bearing the same  $[(\text{bpy})\text{IrCp}^*\text{Cl}]^+$  and  $[(\text{ppy})\text{IrCp}^*\text{Cl}]$  active moieties, respectively.<sup>104</sup> Both MOFs showed catalytic activities towards cerium(IV) driven water oxidation, yet partial decomposition of the iridium complexes was also observed. With a combination of NMR and MS characterization, an iridium species with the formula of  $(\text{H}_2\text{bpy-dc})\text{Ir}(\text{H}_2\text{O})_2\text{XCl}$  (X = acetate or formate) was identified after the recovery of **11** from water oxidation reaction. Further decomposition into  $\text{IrO}_x$  was prohibited by the site isolation in the MOF. This work thus proved that single-site iridium complex is an active water oxidation catalyst and provided important mechanistic insights into water oxidation with molecular catalysts.

Das and coworkers reported incorporation of a molecular water oxidation catalyst,  $\{[\text{Mn}(\text{tpy})]_2(\mu\text{-O})_2\}^{3+}$  (**MnTD**; tpy =

2,2':6',2''-terpyridine), into the MIL-101(Cr)<sup>105</sup> framework.<sup>106</sup> The resulting assembly exhibited slightly lower activity but much enhanced stability compared to the homogeneous solution of the catalyst, which is attributed to prevention of undesired intermolecular interaction between MnTD molecules.

Electrocatalytic water oxidation with MOFs has also been studied, yet the performance is limited by the insulator nature of bulk MOFs. Du and coworkers reported electrocatalytic water oxidation activities of four cobalt-phosphonate coordination polymers in 2013, but they did not rule out the possibility that the catalytic activity could result from cobalt oxide nanoparticles formed from the decomposition of these compounds.<sup>107</sup>

### Concluding remarks

In the past few years, much progress has been made on the design and synthesis of photoactive MOFs based on either metal-organic or organic chromophores. Some of these systems have been tested for degradation of organic pollutants but far fewer systems have been examined in photocatalytic reactions that are relevant to solar fuel production and organic synthesis. Since it is difficult to predict and control the energy levels, lifetimes, and other related properties of the excited states in simple MOFs (such as MOF-5, UiO-66, etc), further development of MOF photocatalysts will likely rely more on the use of well-established photoactive ligands such as porphyrin derivatives, phosphorescent metal complexes, and fluorescent organic compounds.

As many MOFs have modest stability under photocatalytic conditions, recent examples of MOF photocatalysts mainly rely on Zr-carboxylate, Al-carboxylate or Ti-carboxylate SBUs. Although these SBUs are robust enough to survive harsh catalytic conditions, their lack of redox- and photo-activities severely limits the ability to use them as a functional component in a multifunctional photocatalytic system. Expanding the SBU choices to redox- and photo-active metals such as Fe and Co will provide additional opportunities to functionalize both metal connection nodes and bridging ligands to enhance photocatalytic performances of MOFs.

Incorporation of functional moieties such as Pt nanoparticles in MOF channels provides an additional means to endow MOFs with novel functions. Synergistic and cooperative interactions among different functionalities in such a multicomponent MOF open a new strategy for designing molecular materials for photocatalysis and artificial photosynthesis. We foresee that multicomponent MOFs containing diverse and even incompatible functionalities will be assembled to achieve total water splitting or carbon dioxide reduction with energy input from sunlight. MOFs provide an attractive platform to hierarchically organize light-harvesting antenna and catalytic centers to achieve solar energy conversion in a molecular material.

### Acknowledgements

We thank National Science Foundation (DMR-1308229) for financial support.

### Notes and references

<sup>a</sup>Department of Chemistry, University of Chicago, 929 E 57<sup>th</sup> St, Chicago, IL 60637, USA. Email: wenbinlin@uchicago.edu

1. B. O'Regan and M. Gratzel, *Nature*, 1991, **353**, 737-740.
2. M. Gratzel, *Nature*, 2001, **414**, 338-344.
3. D. Gust, T. A. Moore and A. L. Moore, *Accounts Chem. Res.*, 2009, **42**, 1890-1898.
4. S. Y. Reece, J. A. Hamel, K. Sung, T. D. Jarvi, A. J. Esswein, J. J. H. Pijpers and D. G. Nocera, *Science*, 2011, **334**, 645-648.
5. J. Barber, *Chemical Society Reviews*, 2009, **38**, 185-196.
6. W. J. Youngblood, S.-H. A. Lee, K. Maeda and T. E. Mallouk, *Accounts Chem. Res.*, 2009, **42**, 1966-1973.
7. S. Berardi, S. Drouet, L. Francas, C. Gimbert-Surinach, M. Guttentag, C. Richmond, T. Stoll and A. Llobet, *Chemical Society Reviews*, 2014, DOI: 10.1039/C3CS60405E.
8. A. Fujishima and K. Honda, *Nature*, 1972, **238**, 37-38.
9. W. J. Youngblood, S.-H. A. Lee, Y. Kobayashi, E. Hernandez-Pagan, P. G. Hoertz, T. A. Moore, A. L. Moore, D. Gust and T. E. Mallouk, *J. Am. Chem. Soc.*, 2009, **131**, 926-927.
10. T. Ohno, L. Bai, T. Hisatomi, K. Maeda and K. Domen, *J. Am. Chem. Soc.*, 2012, **134**, 8254-8259.
11. X. Wang, Q. Xu, M. Li, S. Shen, X. Wang, Y. Wang, Z. Feng, J. Shi, H. Han and C. Li, *Angewandte Chemie International Edition*, 2012, **51**, 13089-13092.
12. Y. Gao, X. Ding, J. Liu, L. Wang, Z. Lu, L. Li and L. Sun, *J. Am. Chem. Soc.*, 2013, **135**, 4219-4222.
13. J. J. Concepcion, J. W. Jurss, M. K. Brennaman, P. G. Hoertz, A. O. v. T. Patrocinio, N. Y. Murakami Iha, J. L. Templeton and T. J. Meyer, *Accounts Chem. Res.*, 2009, **42**, 1954-1965.
14. T. S. Teets and D. G. Nocera, *Chem Commun*, 2011, **47**, 9268-9274.
15. P. Du and R. Eisenberg, *Energy Environ. Sci.*, 2012, **5**, 6012-6021.
16. D. G. H. Hetterscheid and J. N. H. Reek, *Angewandte Chemie International Edition*, 2012, **51**, 9740-9747.
17. W. Chen, F. N. Rein and R. C. Rocha, *Angewandte Chemie International Edition*, 2009, **48**, 9672-9675.
18. F. Li, Y. Jiang, B. Zhang, F. Huang, Y. Gao and L. Sun, *Angewandte Chemie International Edition*, 2012, **51**, 2417-2420.
19. C. D. Windle and R. N. Perutz, *Coord. Chem. Rev.*, 2012, **256**, 2562-2570.
20. G. S. Engel, T. R. Calhoun, E. L. Read, T.-K. Ahn, T. Mancal, Y.-C. Cheng, R. E. Blankenship and G. R. Fleming, *Nature*, 2007, **446**, 782-786.
21. D. Gust, T. A. Moore and A. L. Moore, *Accounts Chem. Res.*, 2000, **34**, 40-48.
22. H. Imahori, H. Norieda, H. Yamada, Y. Nishimura, I. Yamazaki, Y. Sakata and S. Fukuzumi, *J. Am. Chem. Soc.*, 2000, **123**, 100-110.

23. K. G. Thomas and P. V. Kamat, *Accounts Chem. Res.*, 2003, **36**, 888-898.
24. M. Law, L. E. Greene, J. C. Johnson, R. Saykally and P. Yang, *Nat Mater*, 2005, **4**, 455-459.
25. J.-L. Wang, J. Yan, Z.-M. Tang, Q. Xiao, Y. Ma and J. Pei, *J. Am. Chem. Soc.*, 2008, **130**, 9952-9962.
26. C. Wang and W. Lin, *J. Am. Chem. Soc.*, 2011, **133**, 4232-4235.
27. L. Ma, C. Abney and W. Lin, *Chemical Society Reviews*, 2009, **38**, 1248-1256.
28. J. Lee, O. K. Farha, J. Roberts, K. A. Scheidt, S. T. Nguyen and J. T. Hupp, *Chemical Society Reviews*, 2009, **38**, 1450-1459.
29. M. Yoon, R. Srirambalaji and K. Kim, *Chem. Rev.*, 2012, **112**, 1196-1231.
30. F. Song, C. Wang and W. Lin, *Chem Commun*, 2011, **47**, 8256-8258.
31. D. A. Nicewicz and D. W. C. MacMillan, *Science*, 2008, **322**, 77-80.
32. J. Du and T. P. Yoon, *J. Am. Chem. Soc.*, 2009, **131**, 14604-14605.
33. D. A. Nagib, M. E. Scott and D. W. C. MacMillan, *J. Am. Chem. Soc.*, 2009, **131**, 10875-10877.
34. A. G. Condie, J. C. González-Gómez and C. R. J. Stephenson, *J. Am. Chem. Soc.*, 2010, **132**, 1464-1465.
35. X. Lang, H. Ji, C. Chen, W. Ma and J. Zhao, *Angewandte Chemie International Edition*, 2011, **50**, 3934-3937.
36. C. K. Prier, D. A. Rankic and D. W. C. MacMillan, *Chem. Rev.*, 2013, **113**, 5322-5363.
37. T. Förster, *Annalen der Physik*, 1948, **437**, 55-75.
38. D. L. Dexter, *The Journal of Chemical Physics*, 1953, **21**, 836-850.
39. C. B. Murphy, Y. Zhang, T. Troxler, V. Ferry, J. J. Martin and W. E. Jones, *The Journal of Physical Chemistry B*, 2004, **108**, 1537-1543.
40. M. A. Nasalevich, M. G. Goesten, T. J. Savenije, F. Kapteijn and J. Gascon, *Chem Commun*, 2013, **49**, 10575-10577.
41. C. H. Hendon, D. Tiana and A. Walsh, *Phys Chem Chem Phys*, 2012, **14**, 13120-13132.
42. C. Gomes Silva, I. Luz, F. X. Llabrés i Xamena, A. Corma and H. Garcia, *Chemistry – A European Journal*, 2010, **16**, 11133-11138.
43. A. Fateeva, P. A. Chater, C. P. Ireland, A. A. Tahir, Y. Z. Khimiyak, P. V. Wiper, J. R. Darwent and M. J. Rosseinsky, *Angewandte Chemie International Edition*, 2012, **51**, 7440-7444.
44. C. Wang, K. E. deKrafft and W. Lin, *J. Am. Chem. Soc.*, 2012, **134**, 7211-7214.
45. P. Wu, C. He, J. Wang, X. Peng, X. Li, Y. An and C. Duan, *J. Am. Chem. Soc.*, 2012, **134**, 14991-14999.
46. L. Ma, O. R. Evans, B. M. Foxman and W. Lin, *Inorganic Chemistry*, 1999, **38**, 5837-5840.
47. X. Zhang, M. A. Ballem, Z.-J. Hu, P. Bergman and K. Uvdal, *Angewandte Chemie International Edition*, 2011, **50**, 5729-5733.
48. S. Chen, R.-Q. Fan, C.-F. Sun, P. Wang, Y.-L. Yang, Q. Su and Y. Mu, *Crystal Growth & Design*, 2012, **12**, 1337-1346.
49. C. J. Höller, P. R. Matthes, M. Adlung, C. Wickleder and K. Müller-Buschbaum, *Eur J Inorg Chem*, 2012, **2012**, 5479-5484.
50. H. Zhang, L. Zhou, J. Wei, Z. Li, P. Lin and S. Du, *Journal of Materials Chemistry*, 2012, **22**, 21210-21217.
51. A. Balamurugan, A. K. Gupta, R. Boomishankar, M. Lakshminpathi Reddy and M. Jayakannan, *ChemPlusChem*, 2013, **78**, 737-745.
52. Y.-L. Gai, F.-L. Jiang, L. Chen, Y. Bu, K.-Z. Su, S. A. Al-Thabaiti and M.-C. Hong, *Inorganic Chemistry*, 2013, **52**, 7658-7665.
53. X. Rao, T. Song, J. Gao, Y. Cui, Y. Yang, C. Wu, B. Chen and G. Qian, *J. Am. Chem. Soc.*, 2013, **135**, 15559-15564.
54. M. L. P. Reddy and S. Sivakumar, *Dalton Transactions*, 2013, **42**, 2663-2678.
55. Z. Xia, Q. Wei, Q. Yang, C. Qiao, S. Chen, G. Xie, G. Zhang, C. Zhou and S. Gao, *CrystEngComm*, 2013, **15**, 86-99.
56. J. Xu, L. Jia, N. Jin, Y. Ma, X. Liu, W. Wu, W. Liu, Y. Tang and F. Zhou, *Chemistry – A European Journal*, 2013, **19**, 4556-4562.
57. X.-Q. Zhao, X.-H. Liu, J.-J. Li and B. Zhao, *CrystEngComm*, 2013, **15**, 3308-3317.
58. G. A. Crosby, R. E. Whan and R. M. Alire, *The Journal of Chemical Physics*, 1961, **34**, 743-748.
59. K. Binnemans, *Chem. Rev.*, 2009, **109**, 4283-4374.
60. X. Zhang, Z.-K. Chen and K. P. Loh, *J. Am. Chem. Soc.*, 2009, **131**, 7210-7211.
61. X. Zhang, M. A. Ballem, M. Ahrén, A. Suska, P. Bergman and K. Uvdal, *J. Am. Chem. Soc.*, 2010, **132**, 10391-10397.
62. C. Y. Lee, O. K. Farha, B. J. Hong, A. A. Sarjeant, S. T. Nguyen and J. T. Hupp, *J. Am. Chem. Soc.*, 2011, **133**, 15858-15861.
63. S. Jin, H.-J. Son, O. K. Farha, G. P. Wiederrecht and J. T. Hupp, *J. Am. Chem. Soc.*, 2013, **135**, 955-958.
64. L. Sun, H. Xing, Z. Liang, J. Yu and R. Xu, *Chem Commun*, 2013, **49**, 11155-11157.
65. C. A. Kent, B. P. Mehl, L. Ma, J. M. Papanikolas, T. J. Meyer and W. Lin, *J. Am. Chem. Soc.*, 2010, **132**, 12767-12769.
66. J. Lin, X. Hu, P. Zhang, A. Van Rynbach, D. N. Beratan, C. A. Kent, B. P. Mehl, J. M. Papanikolas, T. J. Meyer, W. Lin, S. S. Skourtis and M. Constantinou, *The Journal of Physical Chemistry C*, 2013, **117**, 22250-22259.
67. C. A. Kent, D. Liu, L. Ma, J. M. Papanikolas, T. J. Meyer and W. Lin, *J. Am. Chem. Soc.*, 2011, **133**, 12940-12943.
68. C. A. Kent, D. Liu, T. J. Meyer and W. Lin, *J. Am. Chem. Soc.*, 2012, **134**, 3991-3994.
69. H.-J. Son, S. Jin, S. Patwardhan, S. J. Wezenberg, N. C. Jeong, M. So, C. E. Wilmer, A. A. Sarjeant, G. C. Schatz, R. Q. Snurr, O. K. Farha, G. P. Wiederrecht and J. T. Hupp, *J. Am. Chem. Soc.*, 2013, **135**, 862-869.
70. C. A. Kent, D. Liu, A. Ito, T. Zhang, M. K. Brennaman, T. J. Meyer and W. Lin, *Journal of Materials Chemistry A*, 2013, **1**, 14982-14989.

71. M. C. So, S. Jin, H.-J. Son, G. P. Wiederrecht, O. K. Farha and J. T. Hupp, *J. Am. Chem. Soc.*, 2013, **135**, 15698-15701.
72. Y. Shi, R. B. M. Hill, J.-H. Yum, A. Dualeh, S. Barlow, M. Grätzel, S. R. Marder and M. K. Nazeeruddin, *Angewandte Chemie International Edition*, 2011, **50**, 6619-6621.
73. A. R. Ramya, D. Sharma, S. Natarajan and M. L. P. Reddy, *Inorganic Chemistry*, 2012, **51**, 8818-8826.
74. H. Li, M. Eddaoudi, M. O'Keeffe and O. M. Yaghi, *Nature*, 1999, **402**, 276-279.
75. P. Horcajada, S. Surble, C. Serre, D.-Y. Hong, Y.-K. Seo, J.-S. Chang, J.-M. Greneche, I. Margiolaki and G. Férey, *Chem Commun*, 2007, 2820-2822.
76. C. Serre, F. Millange, C. Thouvenot, M. Nogues, G. Marsolier, D. Louer and G. Férey, *J Am Chem Soc*, 2002, **124**, 13519-13526.
77. M. Alvaro, E. Carbonell, B. Ferrer, F. X. Llabrés-i-Xamena and H. Garcia, *Chemistry – A European Journal*, 2007, **13**, 5106-5112.
78. i. X. Llabrés, A. Corma and H. Garcia, *The Journal of Physical Chemistry C*, 2007, **111**, 80-85.
79. J.-J. Du, Y.-P. Yuan, J.-X. Sun, F.-M. Peng, X. Jiang, L.-G. Qiu, A.-J. Xie, Y.-H. Shen and J.-F. Zhu, *Journal of hazardous materials*, 2011, **190**, 945-951.
80. K. G. M. Laurier, F. Vermoortele, R. Ameloot, D. E. De Vos, J. Hofkens and M. B. J. Roeffaers, *J. Am. Chem. Soc.*, 2013, **135**, 14488-14491.
81. L.-L. Wen, F. Wang, J. Feng, K.-L. Lv, C.-G. Wang and D.-F. Li, *Crystal Growth & Design*, 2009, **9**, 3581-3589.
82. M. C. Das, H. Xu, Z. Wang, G. Srinivas, W. Zhou, Y.-F. Yue, V. N. Nesterov, G. Qian and B. Chen, *Chem Commun*, 2011, **47**, 11715-11717.
83. X. Wang, Y. Wang, G. Liu, A. Tian, J. Zhang and H. Lin, *Dalton Transactions*, 2011, **40**, 9299-9305.
84. F. Wang, X. Ke, J. Zhao, K. Deng, X. Leng, Z. Tian, L. Wen and D. Li, *Dalton Transactions*, 2011, **40**, 11856-11865.
85. J. Guo, J. Yang, Y.-Y. Liu and J.-F. Ma, *CrystEngComm*, 2012, **14**, 6609-6617.
86. W.-Q. Kan, B. Liu, J. Yang, Y.-Y. Liu and J.-F. Ma, *Crystal Growth & Design*, 2012, **12**, 2288-2298.
87. L. Wen, J. Zhao, K. Lv, Y. Wu, K. Deng, X. Leng and D. Li, *Crystal Growth & Design*, 2012, **12**, 1603-1612.
88. S. Zhou, Z.-G. Kong, Q.-W. Wang and C.-B. Li, *Inorganic Chemistry Communications*, 2012, **25**, 1-4.
89. P. Du, Y. Yang, J. Yang, B.-K. Liu and J.-F. Ma, *Dalton Transactions*, 2013, **42**, 1567-1580.
90. Z. Zhang, J. Yang, Y.-Y. Liu and J.-F. Ma, *CrystEngComm*, 2013, **15**, 3843-3853.
91. S. Zhang, L. Han, L. Li, J. Cheng, D. Yuan and J. Luo, *Crystal Growth & Design*, 2013, **13**, 5466-5472.
92. J. Gao, J. Miao, P.-Z. Li, W. Y. Teng, L. Yang, Y. Zhao, B. Liu and Q. Zhang, *Chem Commun*, 2014. doi: 10.1039/c3cc49440c.
93. C. Wang, Z. Xie, K. E. deKrafft and W. Lin, *J. Am. Chem. Soc.*, 2011, **133**, 13445-13454.
94. M.-H. Xie, X.-L. Yang, C. Zou and C.-D. Wu, *Inorganic Chemistry*, 2011, **50**, 5318-5320.
95. H. K. Chae, J. Kim, O. D. Friedrichs, M. O'Keeffe and O. M. Yaghi, *Angewandte Chemie International Edition*, 2003, **42**, 3907-3909.
96. E. Y. Lee, S. Y. Jang and M. P. Suh, *J. Am. Chem. Soc.*, 2005, **127**, 6374-6381.
97. J. H. Cavka, S. Jakobsen, U. Olsbye, N. Guillou, C. Lamberti, S. Bordiga and K. P. Lillerud, *J. Am. Chem. Soc.*, 2008, **130**, 13850-13851.
98. D. Sun, Y. Fu, W. Liu, L. Ye, D. Wang, L. Yang, X. Fu and Z. Li, *Chemistry – A European Journal*, 2013, **19**, 14279-14285.
99. Y. Fu, D. Sun, Y. Chen, R. Huang, Z. Ding, X. Fu and Z. Li, *Angewandte Chemie International Edition*, 2012, **51**, 3364-3367.
100. Y. Kataoka, K. Sato, Y. Miyazaki, K. Masuda, H. Tanaka, S. Naito and W. Mori, *Energy Environ. Sci.*, 2009, **2**, 397-400.
101. S. Pullen, H. Fei, A. Orthaber, S. M. Cohen and S. Ott, *J. Am. Chem. Soc.*, 2013, **135**, 16997-17003.
102. K. S. Park, Z. Ni, A. P. Côté, J. Y. Choi, R. Huang, F. J. Uribe-Romo, H. K. Chae, M. O'Keeffe and O. M. Yaghi, *Proceedings of the National Academy of Sciences*, 2006, **103**, 10186-10191.
103. S. Wang, W. Yao, J. Lin, Z. Ding and X. Wang, *Angewandte Chemie International Edition*, 2014, **53**, 1034-1038.
104. C. Wang, J.-L. Wang and W. Lin, *J. Am. Chem. Soc.*, 2012, **134**, 19895-19908.
105. G. Férey, C. Mellot-Draznieks, C. Serre, F. Millange, J. Dutour, S. Surblé and I. Margiolaki, *Science*, 2005, **309**, 2040-2042.
106. B. Nepal and S. Das, *Angewandte Chemie International Edition*, 2013, **52**, 7224-7227.
107. Y. Liu, S.-X. Guo, A. M. Bond, J. Zhang and S. Du, *Electrochimica Acta*, 2013, **101**, 201-208.

**Teng Zhang** obtained his BS degree from Peking University, China in 2010 and is currently a graduate student at the University of Chicago under the guidance of Prof. Wenbin Lin. His research focuses on developing porous metal-organic frameworks for heterogeneous asymmetric catalysis and solar energy utilization.



**Wenbin Lin** is James Franck Professor of chemistry at the University of Chicago. His research efforts focus on designing novel molecular materials for sustainability and human health. His group has worked on a variety of research areas, including optical materials, porous materials for catalysis and separation, solar fuels, and nanomedicine. Dr. Lin's group has published over 225 peer-reviewed papers, and his work has been widely cited by the scientific community (Group website: <http://linlab.uchicago.edu>).



**TOC entry:**

This article reviews the latest progress on light-harvesting, organic photocatalysis, proton and CO<sub>2</sub> reduction, and water oxidation using MOFs.

